Available online at www.sciencedirect.com
ScienceDirect
ELSEVIER
International Journal of Rock Mechanics & Mining Sciences 44 (2007) 739–757
International Journal of Rock Mechanics and Mining Sciences
www.elsevier.com/locate/ijrmms

Computer simulation of hydraulic fractures

J. Adachi[a], E. Siebrits[b], A. Peirce[c,*], J. Desroches[d]

[a]Schlumberger Data and Consulting Services, Houston, Texas, USA
[b]Schlumberger Integrated Productivity and Conveyance Center, Sugar Land, Texas, USA
[c]Department of Mathematics, University of British Columbia, Vancouver, Canada
[d]Schlumberger Riboud Product Center, Clamart, France

Received 7 November 2006; accepted 16 November 2006
Available online 5 February 2007

Abstract

We provide a brief historical background of the development of hydraulic fracturing models for use in the petroleum and other industries. We discuss scaling laws and the propagation regimes that control the growth of hydraulic fractures from the laboratory to the field scale. We introduce the mathematical equations and boundary conditions that govern the hydraulic fracturing process, and discuss numerical implementation issues including: tracking of the fracture footprint, the control of the growth of the hydraulic fracture as a function of time, coupling of the equations, and time-stepping schemes. We demonstrate the complexity of hydraulic fracturing by means of an application example based on real data. Finally, we highlight some key areas of research that need to be addressed in order to improve current models.

Keywords: Hydraulic fracturing; Numerical models; Computer simulations

Dedicated to Charles Fairhurst in his 75th year. Of Charles, we can repeat what Ptolemy said about his great teacher, Hipparchus: "a labor-loving and truth-loving man." [1].

1. Introduction

Hydraulic fracturing can be broadly defined as the process by which a fracture initiates and propagates due to hydraulic loading (i.e., pressure) applied by a fluid inside the fracture [1]. Examples and applications of hydraulic fracturing are abundant in geomechanics. Magma-driven dykes can be considered as natural examples, usually on the scale of tens of kilometers [2–4]. On the application side, fracturing of oil and gas reservoirs using a mixture of viscous hydraulic fluids and sorted sand (proppant) is the most commonly used reservoir stimulation technique [31]. Other applications of hydraulic fracturing include the disposal of waste drill cuttings underground [5], heat production from geothermal reservoirs [6], goafing [7] and fault reactivation [8] in mining, and the measurement of *in situ* stresses [108,9].

Even in its most basic form, hydraulic fracturing is a complicated process to model, as it involves the coupling of at least three processes: (i) the mechanical deformation induced by the fluid pressure on the fracture surfaces; (ii) the flow of fluid within the fracture; and (iii) the fracture propagation. Usually, the solid (rock) deformation is modeled using the theory of linear elasticity, which is represented by an integral equation that determines the non-local relationship between the fracture width and the fluid pressure. The fluid flow is modeled using lubrication theory, represented by a non-linear partial differential equation that relates the fluid flow velocity, the fracture width and the gradient of pressure. The criterion for fracture propagation, on the other hand, is usually given by the conventional energy-release rate approach of linear elastic fracture mechanics (LEFM) theory (i.e., the fracture propagates if the stress intensity factor at the tip matches the rock toughness).

*Corresponding author.
E-mail address: anthony.peirce@gmail.com (A. Peirce).

1365-1609/$ - see front matter © 2006 Elsevier Ltd. All rights reserved.
doi:10.1016/j.ijrmms.2006.11.006

Additional complications to this already challenging coupled problem can be easily envisaged by taking into consideration the conditions in which "real" hydraulic fractures occur; for example, the presence of layers of different types of rock (even if these layers are assumed to be parallel); changes in magnitude and/or orientation of the *in situ* confining stresses; the presence of a nearby free surface (of importance in the modeling of magma-driven dykes and in caving applications in mining); the leak-off of fracturing fluid from the fracture to the surrounding rock (or the invasion of reservoir fluid from the rock into the fracture), which is a history-dependent process; the effects of shear and temperature on the fracturing fluid rheology; the transport of suspended proppant particles within the fracture (of primary importance for oil and gas reservoir stimulations), and modeling of fracture recession and closure (due to termination of pumping, forced flowback, or rapid geometric changes in one region as fractures herniate into other lower stress zones).

In this paper, we focus on the modeling of hydraulic fracturing treatments for the stimulation of hydrocarbon reservoirs. The reasons are twofold. First, it is the area of expertise of the authors. Second, over the past 50 years, most of the research effort in hydraulic fracturing has been driven by the needs of the petroleum industry. In what follows, we give a brief historical overview of the development of hydraulic fracturing simulators for use in the petroleum industry, introduce the mathematical equations used to describe the process, discuss numerical implementation issues, benchmarking of solutions, and field applications.

2. Historical background

2.1. Techniques and applications of hydraulic fracturing

In the oil and gas industry, hydraulic fracturing began in the 1930s [10] when Dow Chemical Company discovered that downhole fluid pressures could be applied to crack and deform the formation rock, thereby allowing more effective acid stimulation. Prior to that, a U.S. patent [11] on matrix acidizing referred to pumping fluid under pressure to force acid further into the rock.[1] In the late 1800s and early 1900s, wells were stimulated using nitro-shot if needed. The first hydraulic fracturing treatment to stimulate well production was performed in Kansas in 1947 on a gas well in the Hugoton field in order to compare with the current technology of acidizing wells [13].

Today, hydraulic fracturing is used extensively in the petroleum industry to stimulate oil and gas wells in order to increase their productivity. Thousands of treatments are successfully pumped each year in very diverse geological settings. For example, treatments are routinely injected in: low permeability gas fields; weakly consolidated offshore sediments such as in the Gulf of Mexico; "soft" coal beds for methane extraction; naturally fractured reservoirs; and geometrically complex structures such as lenticular formations.

A "typical" hydraulic fracturing treatment starts with the creation of an initial path for the fracture. This is usually achieved by a technique called "perforation" in which specially designed shaped-charges are blasted on the wellbore walls with given orientations, perforating the casing and creating finger-like holes or weak points in the hydrocarbon-laden formation. A viscous fluid is pumped inside the wellbore, inducing a steep rise in the pressure which eventually leads to the initiation of a fracture at the perforated interval. A "pad" of clean fluid is usually pumped first, to provide sufficient fracture width for the proppant that follows. Proppant is injected at a later stage as a suspension or slurry. The treatment usually takes place on a time-scale of tens of minutes to a few hours, depending upon the designed fracture size and volume of proppant to be placed. At the end of the treatment, when pumping stops, leak-off of the residual fracturing fluid into the porous reservoir allows the fracture surfaces to close onto the proppant pack under the action of the far-field compressive stresses. A conductive packed conduit is formed, and there are additional modeling considerations related to efficient clean-up of the viscous fracturing fluid out of the fracture to allow the oil and/or gas to flow productively, as well as issues related to potential unstable flow-back of proppant and/or reservoir formation particles into the wellbore.

There is a rising tide of evidence from direct monitoring of actual field treatments that suggests that the fracture can grow in a complicated manner, taking advantage of local heterogeneities, layering, and natural fracture networks in the reservoir. These factors complicate the design of treatments and make numerical modeling far more challenging. Furthermore, many hydraulic fracturing operations are performed in so-called "soft" formations, such as weakly consolidated sandstones that are prone to non-linear mechanical failure—a real challenge for current models that are based on the principles of LEFM.

2.2. Hydraulic fracturing models

The development of the first simplified theoretical models started in the 1950s [14–18]. One of the ground-breaking papers to be published in this area was that of Perkins and Kern [19] who adapted the classic Sneddon plane strain crack solution [20] to develop the so-called PK model (see Fig. 1). Later, Nordgren [21] adapted the PK model to formulate the PKN model, which included the effects of fluid loss. Khristianovic and Zheltov [18], and Geertsma and de Klerk [22] independently developed the

[1] One of the first recorded applications of both fluid- and air-driven fracturing for industrial purposes was the quarrying of granite blocks in the Mount Airy region, North Carolina. A description, circa 1910, can be found in [12]. The authors acknowledge Andrew Bunger for finding this possibly oldest reference to an industrial application of hydraulic fracturing published in a journal.

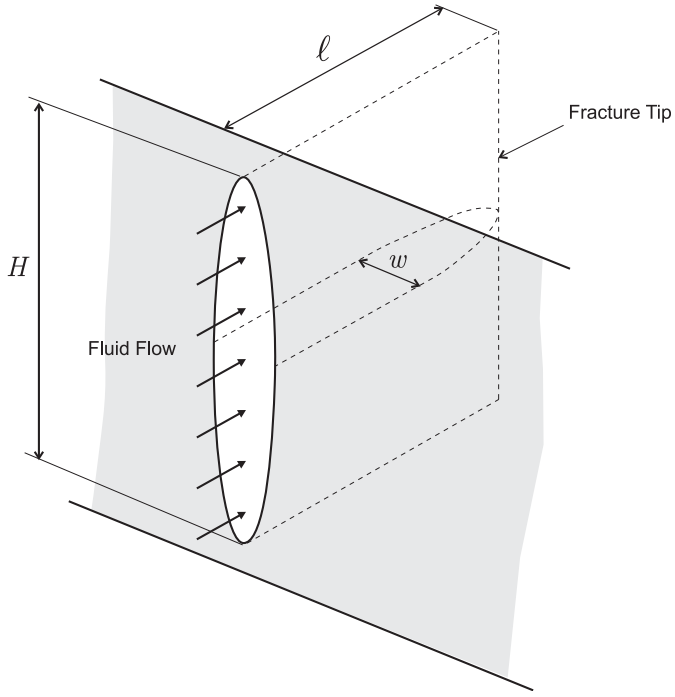

Fig. 1. Schematic showing PKN fracture geometry.

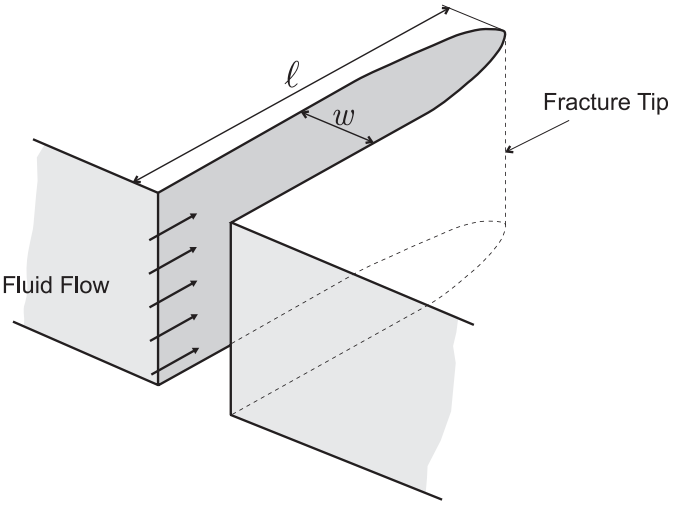

Fig. 2. Schematic showing KGD fracture geometry.

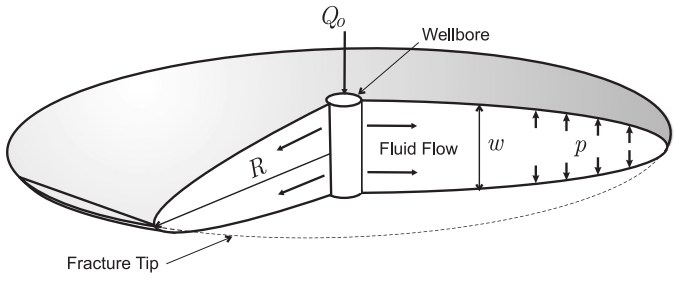

Fig. 3. Schematic showing radial fracture geometry.

so-called KGD (plane strain) model (see Fig. 2). The radial or penny-shaped model (see Fig. 3) with constant fluid pressure was solved by Sneddon [23]. The problem of a flat elliptical crack under constant loading (either far-field stress or internal pressure) was studied by Green and Sneddon [24].

The PKN model is applicable to long fractures of limited height and elliptical vertical cross-section, whereas the KGD model for width calculation is height independent, and is used for short fractures where plane strain assumptions are applicable to horizontal sections. The radial model is applicable in homogeneous reservoir conditions where the injection region is practically a point source (e.g., when well orientation is in the direction of the minimum confining stress or when the fluid is injected from a short perforated section into a reservoir layer that can be considered infinite compared to the size of the fracture). Daneshy [25] extended the KGD model for the case of power-law fluids, and Spence and Sharp [26] properly introduced toughness into the model. Variations of the KGD, PKN and radial models were used routinely for treatment designs as recently as the 1990s, and are still sometimes used today, although they have been largely replaced by the so-called pseudo-3D (P3D) models that are described in more detail below.

Initially, fracturing treatments consisted of injecting a small volume of fluid (VOF) to test the integrity of the wellbore and to "break-down the formation." This was followed by several thousand gallons of proppant-laden slurry. Models were not used in treatment design but production increases were generally significant, although a large number of treatments resulted in premature proppant bridging or "screen-outs." It was nearly a decade (1960–1970) before the simple fracture width models (KGD and PKN) were used to estimate the pad volume required to obtain adequate fracture width to allow proppant entry. During this period, Howard and Fast [27] introduced a method using fracturing fluid loss parameters to calculate fracture penetration. Simple computer models were later developed using the KGD and PKN geometries with proppant transport. These served as guides in the treatment design and provided a method to show the sensitivity to critical input parameters of injection rate, treatment volumes, fluid viscosity and leak-off, and provided a basis for changing these parameters to increase the propped fracture penetration and also to minimize proppant bridging and screen-outs.

In the mean time, the size of treatments increased significantly. In the late 1970s, the price of oil and gas increased, which made it economically viable to exploit low permeability formations. Some wells required massive treatments (in the range of hundreds of thousand of gallons of fluid and up to a million pounds of proppant). The relative cost of these fracture treatments to the total well cost increased from 10% to 50%. These large treatments pointed out the deficiencies in the current

models, and justified more research in fracture modeling. The existing models were not applicable to layered reservoirs where the fracture footprint is sensitive to changes in confining stress across layer interfaces. In such cases, the prediction of fracture height growth requires algorithms that can predict the growth of a fracture through layers containing dissimilar confining stresses. Thus, for example, Simonson et al. [28] developed a symmetric three-layer height growth solution to allow modeling of fracture height as a function of pressure into zones of higher confining stress. This fundamental improvement in the PKN-type models was instrumental in improving the interpretation of fracturing pressures [29]. Fung et al. [30] extended Simonson et al.'s concept to non-symmetric multi-layer cases.

P3D models were developed in the 1980s, and extended the work of Simonson et al. to multiple layers. P3D models are a crude, yet effective, attempt to capture the physical behavior of a planar 3D hydraulic fracture at minimal computational cost. There are two categories: cell-based, and lumped models [31]. In the lumped approach, the fracture geometry at each time step consists of two half-ellipses joined at their centers in the fracture length direction. The fracture length, top tip (top half-ellipse), and bottom tip (bottom half-ellipse) are calculated at each time step (see Fig. 4). Fluid flow follows pre-determined streamlines from the perforated interval to the edges of the ellipse (or may even be 1D along the fracture length direction). In the cell-based approach, the fracture length is sub-divided into a series of PKN-like cells, each with its own computed height (see Fig. 5). P3D models are built on the basic assumption that the reservoir elastic properties are homogeneous, and averaged over all layers containing the fracture height. Since confining stress dominates elastic properties when computing fracture width, this assumption is reasonable in many cases.

The 1980–2000 period saw the development of planar 3D (PL3D) models. These models assume that the fracture footprint and the coupled fluid flow equation are described by a 2D mesh of cells, typically a moving triangular mesh [32–36] (see Fig. 6) or a fixed rectangular mesh [37,38] (see Fig. 7), oriented in a (vertical) plane. The full 3D elasticity equations are used to describe the fracture width as a function of fluid pressure. PL3D models are more accurate and computationally far more expensive than P3D ones.

The need for PL3D models arose because there are specific types of fracture treatments that P3D models are not suited to model. For example, when the layer confining stresses vary non-monotonically as a function of depth, or when unconfined height growth occurs, P3D models tend to break down numerically. Any layered reservoir that results in an hour-glass shaped fracture footprint (e.g.,

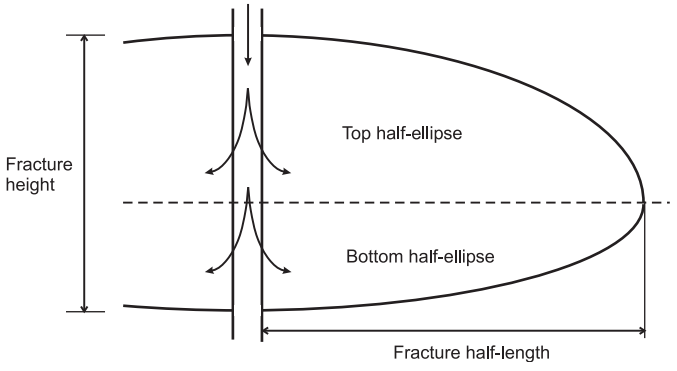

Fig. 4. Schematic showing fracture geometry based on pseudo 3D lumped elliptical model.

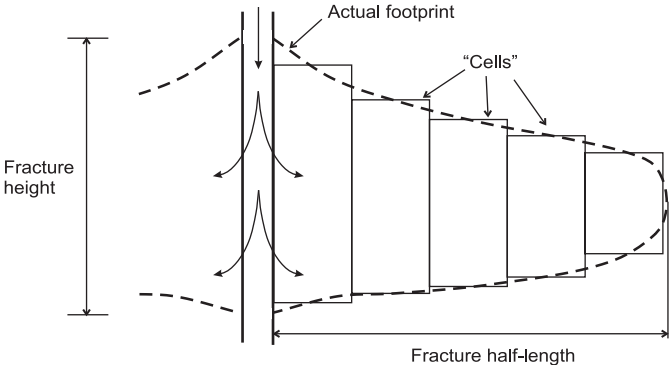

Fig. 5. Schematic showing cell-based pseudo-3D fracture geometry.

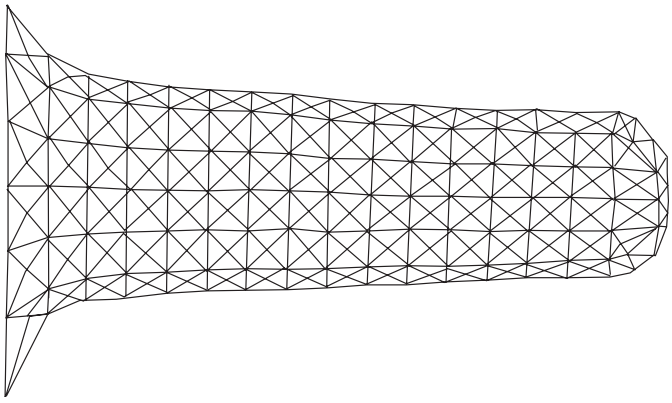

Fig. 6. Schematic showing planar 3D fracture geometry based on moving mesh system of triangular elements.

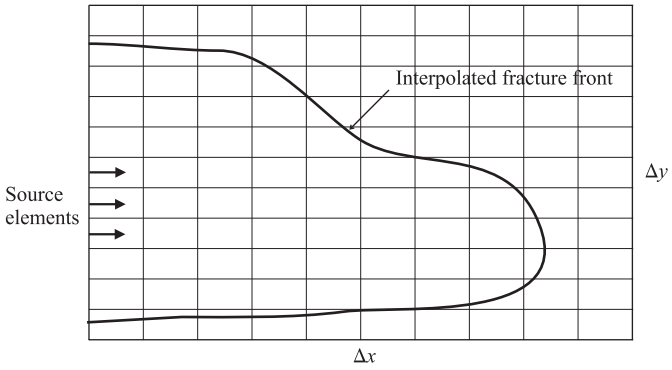

Fig. 7. Schematic showing planar 3D fracture geometry based on regular (fix) system of quadrangular elements.

where the middle layer of a three-layer system is "stiffer" and more likely to "pinch" the fracture width) is not suited to a P3D model. In many reservoirs, the pay zones are located in less competent sandstones, prone to mechanical failure due to production-induced pore pressure changes. In such cases, indirect vertical fracturing can be used to reduce the risk of sanding. The perforated interval is selected to be in an adjacent more competent layer. The fracture initiates in this layer and then grows, by design, up or down into the less competent pay zone containing the bulk of the fracture.

There have also been attempts to model fully 3D hydraulic fractures [39] with limited success. The computational burden on such coupled systems is still excessive, even with today's powerful computational resources. There are also unresolved physical questions pertaining to the generation and spacing of mode III fractures that such models do not currently address.

2.3. Scaling laws and propagation regimes

In recent years, there has been a return to fundamental research, with significant effort being devoted to understanding the different regimes of propagation in hydraulic fracturing. The objective of this research has been to gain insight into the properties of the classical hydraulic fracture models rather than to develop new models to deal with the complex and challenging new environments in which hydraulic fractures are being developed. This work was developed on two fronts. First, an exhaustive analysis of the near-tip processes (using methods based on asymptotic theory) was undertaken, which has significantly extended the pioneering results of [40] for the zero-toughness, impermeable case; and of [41] for the zero-toughness, leak-off dominated case. This ongoing effort has accomplished not only the inclusion of toughness and fluid lag, but also the development of all the pertinent intermediate asymptotic regimes [42–44].

The second front includes the analysis of the dominant dimensionless groups that control the hydraulic fracturing process [45,46]. This work has shown that hydraulic fractures can be categorized within a parametric space, whose extremes are controlled by leak-off, toughness, or viscosity dominated processes. In general, a hydraulic fracture evolves with time within this parametric space, following trajectories that are determined by the rock properties (elastic moduli, toughness, leak-off coefficient), fluid viscosity, and injection rate.

Within this framework, semi-analytical and numerical solutions have been developed for simple geometries (KGD and penny-shaped) for different asymptotic regimes, such as zero toughness impermeable [47–49]; small toughness impermeable [50]; finite toughness impermeable [51,26]; large toughness impermeable [52,49]; zero toughness permeable [53] regime; and finite toughness permeable [54] regime solutions. These solutions have not only yielded an understanding of the evolution of hydraulic fractures in and between different propagation regimes, but have also provided useful benchmarks for numerical simulators.

Another important consequence of this research work is that the newly developed scaling laws can be used to define the range of parameters required to properly model the growth of a hydraulic fracture at the field or laboratory scale, or at least to properly interpret and extrapolate experimental data. For example, in most field-scale treatments, the dominant factor that controls hydraulic fracture growth is viscosity, and not toughness (the latter quantity has been historically used to assign fracture growth control in hydraulic fracturing simulators). However, in laboratory tests, where block sizes of 1 cubic foot are typical, toughness is the controlling mechanism, even when highly viscous fluids are injected. Hence, direct application of experimental results to field scale may lead to misleading conclusions. Recent experimental results [55–57] have provided physical evidence of the validity of these similarity solutions. The scaling law methodology was crucial in identifying the appropriate ranges of parameters in order to design the experiments to capture these different physical solutions.

3. Mathematical equations

3.1. Underlying assumptions

Fig. 8 is a schematic of a typical hydraulic fracturing problem that is of interest (in this case a PL3D situation is depicted). The reservoir consists of multiple layers, each with distinct properties such as elastic moduli, toughness, permeability, porosity, and confining stress, extracted from log data, seismic surveys, and/or down-hole stress tests.

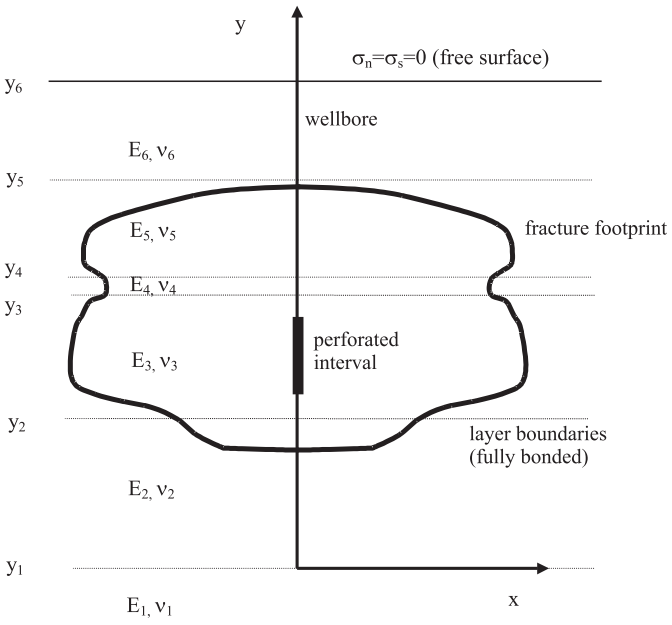

Fig. 8. Schematic of a multi-layered reservoir showing footprint of a planar 3D fracture oriented vertically. In the figure, y_1–y_6 are layers with different elastic moduli and Poisson's ratios.

Layer interfaces are generally assumed to be parallel to each other, although in reality, more complex situations do occur. A thoroughly comprehensive model, aside from being impracticable, would contradict the main purpose of a numerical model—to represent the essential mechanism in an approximate manner so as to aid understanding and design while remaining computationally feasible [58].

The basic equations governing a hydraulic fracturing model are: (a) the elasticity equation (expressing the mechanical response of the host reservoir to the loading imposed on the propagating fracture surfaces by the pressure due to the injected fluid); (b) the fluid flow equation (expressing the conservation of fluid mass, which yields the velocity field of the fluid inside the fracture); (c) the leak-off term (describing the history-dependent loss of the injected fluid from the fracture into the porous reservoir, due to a positive pressure gradient between the fluid-filled fracture and the reservoir); (d) the proppant transport equation (describing the time-dependent distribution of the concentration of proppant in the fracture); (e) the fracture growth condition (that controls the rate and manner of growth of the hydraulic fracture, typically based on the assumptions of LEFM).

All of these equations must be properly coupled together in a stable, robust, and efficient manner to generate the solution for the moving boundary problem—comprising: the fracture footprint, the fracture width, the fluid pressure, and the proppant concentration as functions of time and space. The following assumptions are typically made when building numerical hydraulic fracturing models: (a) the host reservoir material is considered to be linear elastic; (b) in the case of a multi-layered reservoir, the layer interfaces are assumed to lie parallel to each other and to be perfectly bonded (geological stress variations and even jumps across layer interfaces can easily be modeled while a layered Green's function approach [59,60] can be used to model elastic moduli that are piecewise constant); (c) the hydraulic fracture is (usually) assumed to lie in a single vertical plane; (d) the fluid flow in the fracture obeys Poiseuille flow and is incompressible, and sequential injections of multiple fluids are immiscible.

In addition to plastic behavior of the host rock, non-parallel and debonded interfaces, and non-planar fractures, these models typically ignore the following additional effects: (a) the actual reservoir may be naturally fractured; (b) the actual reservoir may contain a heterogeneous stress field due to poroelastic influences of neighboring producing wells; (c) usually, the fluid flow equations are restricted to relatively simple models for the fluid rheology, such as Newtonian or power-law. However, actual fluids used for hydraulic fracturing treatments have more complicated rheologies (yield stresses, viscoelasticity, etc.); (d) leak-off is often assumed to be uncoupled from the fluid pressure, and to be restricted to the linear (1D) flow regime; (e) many effects related to the modeling of proppant transport (e.g., interaction and collision between proppant particles, shear-induced proppant migration, proppant settling, etc.) are often modeled in a rather simplistic manner, or neglected altogether.

3.2. Elasticity equations

The elasticity equations are used to calculate the fracture widths due to the net pressures (local fluid pressure minus local confining stress) at each point on the fracture footprint. The elasticity equations in 3D (a similar expression can be obtained in the 2D case) can be written [59,60] as an integral equation of the form:

$$Cw = \int_{\Omega(t)} C(x,y;\xi,\eta)\; w(\xi,\eta,t)\,\mathrm{d}\xi\,\mathrm{d}\eta = p(x,y,t) - \sigma_c(x,y), \tag{1}$$

where p is the fluid pressure inside the fracture, σ_c is the local minimum *in situ* (or confining) stress, and w is the fracture width. The non-local kernel function C contains all the information about the layered elastic medium. It is assumed that the fracture occupies the region denoted by $\Omega(t)$ at time t.

It is possible that $p<\sigma_c$ within certain subregions of the fracture footprint $\Omega(t)$. Depending on the relative magnitude of p and σ_c as well as the extent of these so-called pinched regions, it is possible that the corresponding width determined by Eq. (1) can be negative. Since such an interpenetration of the fracture surfaces is physically impossible, it is necessary to impose a minimum constraint w_c on the width

$$w \geqslant w_c. \tag{2}$$

We permit $w_c>0$ because surface roughness prevents complete mechanical closure of a fracture, thus allowing fluid to continue to flow.

There are essentially two main choices when discretizing the elasticity equations. We can either employ an integral equation formulation such as Eq. (1) known as the displacement discontinuity method [61], or choose to discretize the 3D partial differential equations via the finite element or finite difference methods. If boundary integral schemes are employed, the 3D layered reservoir is assumed to be linear elastic, and the discretized equations (in the case of a PL3D model) can be rigorously reduced to a planar system of elements covering the fracture footprint [59,60]. Other alternatives for layered systems include the use of moduli perturbation [62] or Galerkin-based [63] schemes. If finite element or finite difference schemes are employed to discretize the 3D partial differential equations [31], then a large volume of the reservoir in the vicinity of the hydraulic fracture needs to be discretized in order to compute the fracture widths accurately—a computationally expensive option.

Various approximations for layered reservoirs have been used in commercially available simulators, e.g., [37,64,65]. Ref. [37] erroneously assumes that the spatially varying elastic moduli can be factored out of the integral equation, thus leading to an incorrect formulation. Ref. [65] stacks a

series of bi-layer solutions together to approximate the multi-layer system. Ref. [64] models the multi-layer system in an approximate manner by excluding higher order image terms. The two latter approaches can be prone to errors in estimation the fracture width when thin layers containing large changes in elastic moduli span the fracture footprint.

Attempts to model multi-layer systems where layers are permitted to frictionally slip have met with limited success. Rigorous models of such layered systems are computationally very expensive [66], and "approximations" [67] that involve non-rigorous changes to the elastic influence matrix in an attempt to control fracture height growth and hence "mimic" fracture growth in the vicinity of frictional interfaces are at best highly approximate and subject to significant errors. This is a topic for further research.

3.3. Fluid flow and leak-off equations

In the case of a planar fracture that grows in a 3D elastic medium, the basic 2D fluid flow equations are governed by the Reynolds' equation given by

$$\frac{\partial w}{\partial t} = \nabla \cdot [D(w)(\nabla p - \rho \mathbf{g})] + \delta(x,y)Q, \tag{3}$$

where ρ is the fluid density, $\mathbf{g}$ is the gravity vector, $\delta(\cdot)$ is the Dirac delta function, $Q = Q(x,y,t)$ is the source injection rate (we note that line sources may also be defined to represent perforated intervals along the wellbore), $D(w) = w^3/12\mu$, and μ is the Newtonian fluid viscosity. The addition of a leak-off sink term and a power-law fluid yields

$$\frac{\partial w}{\partial t} = \nabla \cdot [D(w,p)(\nabla p - \rho \mathbf{g})] + \delta(x,y)Q - \frac{2C_L}{\sqrt{t - t_0(x,y)}} - 2S_0\delta(t - t_0(x,y)), \tag{4}$$

where C_L is the Carter leak-off coefficient having dimensions $[LT^{-1/2}]$ [16], $t_0(x,y)$ is the initiation time for the leak-off (i.e., the time at which the fracture front first reaches the coordinate (x,y)), and

$$D(w,p) = N' w^{(2n'+1)/n'} |\nabla p - \rho\, \mathbf{g}|^{(1-n')/n'}, \tag{5}$$

$$N' = \left(\frac{n'}{2n'+1}\right)\left(\frac{1}{2^{n'+1}K'}\right)^{1/n'}, \tag{6}$$

$$|\nabla p - \rho \mathbf{g}| = \sqrt{\left(\frac{\partial p}{\partial x} - \rho\, g_x\right)^2 + \left(\frac{\partial p}{\partial y} - \rho\, g_y\right)^2}, \tag{7}$$

where the power-law exponent n' is typically in the range $0.1 < n' < 2$, K' is the consistency index, g_i are the components of the gravity vector, and the spurt S_0 (which represents a very rapid initial leak-off at early times before a filter cake builds up on the fracture surfaces) has units of $[L^3/L^2]$. For a Newtonian fluid, $n' = 1$ and $K' = \mu$ and we recover the Newtonian pressure gradient terms as per Eq. (3).

The application of the Carter leak-off model to a simulator usually implies that we assume that the leak-off is 1D, in a direction orthogonal to the fracture plane. This approximation is reasonable provided the fracture is propagating sufficiently rapidly that non-orthogonal leak-off is negligible. However, in highly permeable reservoirs, leak-off exhibits a non-orthogonal flowpath—laboratory tests clearly show a zone of leak-off ahead of the main tip of the fracture [68]. In addition, fluid leak-off can be a complex process, and may, depending on the fluid properties, be sensitive to the pressure and the temperature. In some cases, wormhole behavior of the leaking fluid has been noted [69], and the inclusion of such effects in a fracture simulator is challenging. In high permeability reservoirs, ~90% of the injected fluid can leak off into the reservoir during the injection treatment. It is thus important to be able to simulate this process in at least an averaged manner.

The fluid flow equations are usually solved using finite element, finite difference or finite volume [70] schemes. In most hydraulic fracturing models, the fluid flow equations are discretized over the fracture footprint to produce a 2D system of equations where the fluid pressure is the primary unknown. Fracturing fluids include polymers, viscoelastic surfactants, and foams and their rheology is typically approximated to follow a power-law model. As the fracturing fluid advances through the fracture volume, the warmer surrounding reservoir heats it up, and thermal transfer will cause the viscous fluid to thin (i.e., the apparent viscosity decreases and the fluid becomes more Newtonian ($n' \to 1$)); this also needs to be built into the fluid flow simulations. Furthermore, the evolving concentration of proppant particles also causes the rheology of the fluid to adjust. The stiffness terms in the fluid flow equations can thus, in general, be complicated functions of fluid consistency index, power-law index, fracture width, proppant concentration, temperature, and fluid pressure. Proppant-carrying fracturing fluids are designed to be viscous while carrying the proppant, and to eventually "break" (i.e., thin dramatically) after a time delay or when a critical temperature is reached. This ensures that the injected fluid is more easily cleaned up (by flowing back into the wellbore) once the injection has ended and the fracture surfaces have closed onto the packed proppant. Schedules generally contain multiple fluid types, so that a rigorous placement simulator should account for all of the above physical effects.

3.3.1. Boundary conditions

Along the perimeter of the fracture, we specify a zero fluid flux boundary condition given by

$$D(w,p)\mathbf{n} \cdot (\nabla p - \rho \mathbf{g}) = 0, \tag{8}$$

where $\mathbf{n}$ is the outward unit normal along the fracture perimeter. This boundary condition is only applicable if the fluid completely fills the fracture, i.e., if the fluid lag is considered negligible compared to the scale of the fracture. Otherwise, we must alter the equations to account for the

effect of the fluid lag. Indeed, the inclusion of a fluid lag (defined as a cavity between the fracture tip and the fluid front, with practically zero pressure) becomes an additional unknown of the problem [44]. The boundary condition at the fluid front then becomes a zero pressure condition, whereas tracking of the fracture tip (or of the fluid lag length) requires one to account for the fluid lag in the elasticity equation explicitly.

One of the complications of the zero flux boundary condition is that the operator $\nabla \cdot (D(w,p)\nabla \bullet)$ together with this boundary condition is no longer invertible since the solutions are only unique up to an arbitrary constant pressure. This boundary condition introduces several challenges both from a discretization point and for the appropriate coupling algorithm. For example, normal derivative boundary condition implementations along curved boundaries using 2D finite difference methods are extremely tedious if not impracticable. In this case, it is preferable to resort to finite volume or finite element discretization procedures. The pressure indeterminacy for zero flux boundary conditions complicates the coupling algorithm since the appropriate pressure level becomes an unknown of the problem. For situations in which width constraints are not active, this does not pose a problem. However, when width constraints are active in some of the elements, this pressure indeterminacy can become very difficult to resolve.

3.3.2. Conservation of mass and the solvability condition

The solvability condition is a constraint (which simply expresses the global conservation of mass) that needs to be imposed so that a solution to the fluid flow equation along with the derivative boundary conditions exists at all. The solvability condition plays an important role in the design of efficient schemes to solve the coupled elasto-hydrodynamic equations because of the pressure indeterminacy of the fluid flow equation.

To derive the 2D solvability condition,[2] we integrate Eq. (4) over the region $\Omega(t)$ to obtain

$$\int_{\Omega(t)} \frac{\partial w}{\partial t}\,\mathrm{d}V = \int_{\Omega(t)} \left[\nabla \cdot (D(w)\nabla p) + \delta(x,y)Q - \frac{2C_{\mathrm{L}}}{\sqrt{\tau - t_0(x,y)}} - 2S_0\delta(t - t_0(x,y))\right]\mathrm{d}V. \quad (9)$$

Application of Leibnitz's rule and the divergence theorem gives

$$\frac{\partial}{\partial t}\int_{\Omega(t)} w\,\mathrm{d}V = \int_{\partial\Omega(t)} D(w)\frac{\partial p}{\partial \mathbf{n}}\,\mathrm{d}S + Q - \int_{\Omega(t)} \left[\frac{2C_{\mathrm{L}}}{\sqrt{\tau - t_0(x,y)}} + 2S_0\delta(t - t_0(x,y))\right]\mathrm{d}V. \quad (10)$$

[2]For simplicity, we have assumed that the fluid is Newtonian and we have removed the gravity terms—i.e., we assume that the gradient ∇p in the following equations is actually given by $\nabla p - \rho\,\mathbf{g}$.

Using the zero flux boundary conditions for the pressure and integrating with respect to time from the beginning of the pumping process, we obtain the solvability condition

$$\int_{\Omega(t)} w\,\mathrm{d}V = \int_0^t Q(\tau)\,\mathrm{d}\tau - \int_0^t \int_{\Omega(\tau)} \frac{2C_{\mathrm{L}}}{\sqrt{\tau - t_0(x,y)}}\mathrm{d}V\,\mathrm{d}\tau - 2S_0\ \mathrm{Area}[\Omega(t)]. \quad (11)$$

We observe that the solvability condition expresses the global conservation of mass.

3.4. Proppant transport

The transport and placement of proppant within the fracture is usually modeled by representing the slurry (i.e., the mixture of proppant and fluid) as a two-component, interpenetrating continuum. This implies that the fluid flow equations (i.e., conservation of mass and conservation of momentum) are solved for the mixture, and not for each individual component. The distribution of proppant in the fracture is given by its volumetric concentration (defined as the probability of finding a proppant particle at a given point in space and time [71]), which is the additional variable to be determined. In modeling proppant transport and placement, it is often assumed that: (a) both proppant and fluid are incompressible; (b) the proppant particles are small compared to a characteristic lengthscale, in this case the fracture width; and (c) the only mechanism to account for "slip" between the proppant and the carrying fluid is gravity-induced settling, i.e., relative proppant-fluid velocities due to migration by self-diffusion (created by shearing and/or proppant collision), Taylor dispersion, or clustering are usually neglected. This implies that, in the absence of gravity, the proppant and fluid move at the same velocity at any given point.

Assumption (a) implies that the governing equations to describe the flow of slurry can still be derived from principles of fluid dynamics and lubrication theory. Assumption (b) means that we are dealing with a relatively dilute suspension of particles. This assumption, of course, has a limit: in situations with significant leak-off, or after shut-in, the relative concentration of proppant with respect to the fluid can reach significantly larger values, to the point that the mixture would start to behave more like a porous solid. If the concentration reaches a given saturation value (generally determined by geometrical considerations), the proppant particles conform to a "pack," and thereafter, only the fluid phase is able to mobilize through the interstitial pores. In addition, we can expect that near the fracture tips, the fracture width is of the same order of magnitude as the proppant diameter. The mobility of the proppant in this case will rapidly decrease, to the point of stopping altogether in some cases, again forming a "pack" or "bridge." This phenomenon is usually taken into account (albeit in a rather pragmatic way) by setting a minimum fracture width (as an experimentally-derived

proportion of the proppant mean diameter) required for the proppant to circulate freely.

Assumption (c) is probably the weakest foundation of these models, as it is known [71–74] that slumping and migration do occur in shear-induced flow of particle suspensions. The two most important consequences of using this assumption are that: (a) the concentration of proppant across the fracture width can be taken as homogeneous (i.e., there is no layering, banding or "sheet flow"); and (b) by ignoring any Taylor dispersion effects, we can consider the advancing front of proppant as a "sharp" front, without any dispersion ahead.

Modeling of the proppant transport then reduces to solving an advective (mass conservation) equation for the proppant volumetric concentration c given by

$$\frac{\partial(cw)}{\partial t} + \nabla \cdot (cw\mathbf{v}^{\mathrm{p}}) = 0, \tag{12}$$

where $\mathbf{v}^{\mathrm{p}}$ is the proppant velocity vector. If dispersion ahead of the proppant front is neglected, it is desirable to minimize any effects of numerical dispersion, which are common in solving hyperbolic equations like (12) using conventional upwind methods. Usually, this is accomplished by applying a second-order correction with a limiter. The limiters are selected based on the total variation diminishing (TVD) principle [75–77]. The purpose of the limiters is to retain the second-order terms where the solution is smooth and to suppress the second-order terms where the solution has discontinuities. In this way, both the numerical diffusion of the first-order schemes and the dispersion of the second-order schemes are minimized or prevented.

Coupling between Eq. (12) and the rest of the governing equations of the hydraulic fracture model is given by three variables: (a) the slurry density, which affects the fluid flow Eq. (3) as a correction to the pressure gradient; (b) the slurry velocity, which is obtained by solving the fluid flow equations; and (c) the viscosity of the slurry, which is calculated by adjusting the clean fluid viscosity with the proppant concentration by means of empirical formulae. To obtain the velocity of the proppant from the slurry velocity we have to consider the possibility of slip between the fluid and the proppant. The proppant velocity vector is then calculated from the slurry velocity $\mathbf{v}$ using

$$\mathbf{v}^{\mathrm{p}} = \mathbf{v} - (1 - c)\mathbf{v}^{\mathrm{s}}, \tag{13}$$

where $\mathbf{v}^{\mathrm{s}}$ is the slip velocity vector. Specific phenomena associated with the transport of proppant can be included in this velocity. If we consider that slip is assumed to be caused only by settling, this vector is parallel to the gravity acceleration vector $\mathbf{g}$. Usually, the magnitude of the slip velocity $\mathbf{v}^{\mathrm{s}}$ is calculated from variations of the classical Stokes equation. A correction factor (function of the concentration) to take into account the effect of proppant interaction and wall effects ("hindered settling") is applied to the Stokes settling velocity. A review of such equations can be found in [72]. Other models are discussed in [78–80]. Experimental observations are cited in [81].

Regarding the viscosity of the slurry, this is actually one of the most difficult (and critical) aspects of the modeling. Proper formulation of the momentum equation for the problem of a suspension of solid particles yields terms that are related to the interaction between particles and between particles and the fluid. Accounting for these effects in detail is challenging, and most models that attempt to describe these interactions are still awaiting experimental verification [71]. Hence, it is common practice to "lump" all these effects into a modified viscosity of the slurry, which is usually calculated using an expression of the form

$$\mu = \mu_0(1 - c/c_*)^{\beta}, \tag{14}$$

where μ_0 is the effective Newtonian viscosity of the clean fluid, c_* is a saturation concentration,[3] and β is a negative number (usually $-3 < \beta < -1$). The effect of Eq. (14) is to increase the viscosity as the proppant concentration increases. There is some experimental verification [81] for this type of model, although there are a variety of other models that have been postulated [78,82,83]. From the modeling point of view, an adjustment formula like Eq. (14) presents the inconvenience that the effective viscosity increases very rapidly as c approaches c_*. Usually, a threshold value (either in c or in μ) has to be enforced. However, a limitation of Eq. (14) is that, as concentration increases, it is expected that the slurry will start to behave more like a solid than a fluid. Hence, the use of a lubrication-type equation (even with a very high viscosity) to model the slurry transport may become inappropriate.

3.5. Evolution of the fracture front

3.5.1. Meshing strategy

There are essentially two classes of meshing that are typically used in hydraulic fracture models, viz., fixed (Eulerian) or moving (Lagrangian). It is also possible to consider a hybrid approach in which the underlying grid is fixed within the fracture while the location of the fracture front is treated by discrete points that move. This procedure is known as front tracking.

In the case of moving meshes, triangular elements are typically used to define the fracture footprint. This may be constructed in two ways: (a) addition of new elements to advancing sections of the fracture, with periodic re-meshing of the entire fracture footprint to recover more tractable aspect ratios; or (b) re-meshing of the entire fracture footprint at each growth step. Moving meshes are desirable because they allow for the fracture footprint to be

[3]The saturation value c_* is usually given by $c_* = 0.52$ (known as "loose packing," which corresponds to an arrangement of regular spheres in a cubic pattern), or by $c_* = 0.65$ (known as "tight packing," which corresponds to the maximum concentration that can be achieved by random packing of regular spheres).

modeled at a user-defined level of detail at any growth step, i.e., moving meshes can be constructed so that the number of active elements at any growth step stays at a "reasonable" number, hence maintaining good accuracy at early times, and low CPU times and good accuracy at late times. However, moving meshes require interpolation of fracture width, pressure, concentration, and leak-off data for each re-meshing procedure, thereby introducing interpolation errors into the system. In addition, the use of moving meshes becomes problematic in the case of a layered material, where elements may partially cross layer interfaces—the assignment of averaged layer properties over a crossing element will result in polluted results.

Fixed meshes are typically constructed using rectangular elements. Algorithms that employ fixed meshes are easier to encode, and avoid interpolation issues with associated noise in the width and pressure histories. However, resolution issues can affect these algorithms, i.e., too few (many) elements at early (late) times. Re-meshing can also be employed for fixed meshes to make more efficient use of the element count and to reduce CPU times, with concomitant interpolation errors as in the case of moving meshes. In addition, the use of rectangular elements can imply poor (or binary) definition of the fracture front. Since most of the pressure drop occurs near the fracture tip, special care needs to be taken to obtain accurate results in the case of a fixed mesh. One alternative is to sub-mesh near the fracture tip [84], but this is computationally expensive, and again requires interpolation as the fracture front moves and drags the sub-mesh region along with it. Another alternative is to use specially enhanced tip elements [85] to increase the accuracy of the solution, or to force exact tip asymptotic solutions [45] in the tip elements.

In the context of a fixed mesh, efficient methods have been developed to capture the front evolution by tracking the dynamics of an ancillary field variable, which can be used to establish the front position. The VOF method [86] tracks the evolution of the fill fraction, which represents the fraction of a discretization element that is filled with fluid. The level set method [87,88] tracks the front position as the zero level set of a scalar function, which is assumed to evolve on the regular grid according to a hyperbolic conservation law defined by the normal velocity of the front.

3.5.2. Locating the front position

There are a number of approaches that can be used to locate the fracture front in a hydraulic fracturing simulator. These methods can be classed in two main categories: explicit and implicit methods. For explicit methods, key information from the end of the previous growth step is used to predict the advance of the fracture front for the current growth step. Such schemes will generate poor results in the case of fracture growth through multiple layers, because the fracture front advancement can only depend on local conditions at the location of the fracture tip at the end of the previous growth step. These schemes are only effective if the time step is severely restricted in order to reduce such errors. A better alternative is to iterate on the fracture front within the current growth step. Such implicit methods can be combined with level set or VOF methods to iterate on the fluid front to achieve an accurate fracture footprint. However, these methods are expensive since multiple iterations of the coupled system of equations are required before the fracture footprint converges—this is aggravated in layered reservoirs where significant changes in elastic moduli or confining stress can occur from one layer to the next.

3.5.3. Propagation criterion

The propagation criterion for the fracture represents a very special type of tip boundary condition, as it practically dictates the nature of the whole solution. Usually, numerical models consider the conventional LEFM criterion that the fracture propagates (quasi-statically) if $K_I = K_{Ic}$, where K_I is the stress intensity factor (the strength of the inverse square-root stress singularity at the tip) and K_{Ic} is the toughness, a material property of the rock. In most cases, this propagation condition is enforced by using "tip elements" in which the width profiles are prescribed according to the classical square-root shape.

Hydraulic fractures, however, represent a special class of fracturing, due to the coupling between different processes (elastic deformation, rock fracturing, fluid flow in the fracture, leak-off) taking place near the tip. It has been recently recognized that, in this near-tip region, each of these processes can be associated with a characteristic lengthscale [42]. Predominance amongst these lengthscales determines the fracture response (the propagation regime), characterized by the order of the stress (or pressure) singularity. This yields a complex multi-scale solution for the propagation of the fracture. The importance of this type of asymptotic analysis lies in the fact that, even though these solutions are obtained at the scale of the near-tip region, the propagation regime of the whole fracture is actually determined by the tip.

Following this methodology, it can be shown that, for a relatively large range of parameters encountered in field-scale hydraulic fracturing treatments, fracture propagation is actually dominated by viscous dissipation, or by a combination of viscous dissipation and leak-off. In such cases, the classical LEFM stress singularity is restricted to a very small lengthscale (practically negligible from the standpoint of the resolution of numerical simulations) near the tip [50], and other singularities dominate the propagation process. In other words, toughness may become irrelevant.

Thus the indiscriminate use of a tip element based on the classical square-root shaped tip may lead to an incorrect fracture footprint. Recognition of the current propagation regime (and hence of the proper stress and pressure singularities at the tips, or at least at the lengthscale of the discretization) at any point along the outer rim of the

fracture is therefore a significant issue. The use of "smart" tip elements (i.e., tip elements that could adjust the width shape and/or pressure singularity according to the local propagation regime), or enforcement of the "proper" pressure singularity at the tips (i.e., the singularity corresponding to the regime in which most of the fractures are expected to develop), should be part of any field-scale hydraulic fracturing model.

Fluid lag: Further complications can be added by considering, for example, the existence of a lag (of unknown length) between the crack tip and the fluid front. Laboratory experiments have shown that the fluid front and the fracture front do not coincide. Indeed, the fracture can advance ahead of the fluid, in which case there is a "fluid lag," i.e., a dry fracture zone ahead of the fluid front, or behind the fluid, in which case there is an "invaded zone" ahead of the crack tip. Note that it is nearly impossible to ensure that the fracture front and the fluid front will coincide for any length of time. Until recently, hydraulic fracturing treatments were mostly performed in lower permeability formations (<100 mD), and the formation of a fluid lag was likely. Nowadays, treatments are performed in high permeability formations (>1 D) and an invaded zone can occur.

In order to determine the relevance of fluid lag, explicit solution for the size of the fluid lag as part of the solution process is required. Because of the focus on the tip of the fracture, investigators have focused on hydraulic fractures of simple geometries, treating the rock as elastic and later as plastic [89]. It was found that, unless the pore pressure in the reservoir is close to the confining stress σ_c (i.e., the case of an overpressured reservoir where the limit for the pore pressure is actually the confining stress), the presence of a fluid lag was more important than its exact size. Furthermore, the presence of the fluid lag shielded the hydraulic fracture from the effect of the fracture toughness in most practical cases. These results then were extended by Detournay and Garagash [43,44], demonstrating that various regimes could be distinguished and that asymptotic solutions could be derived for each of them, allowing one to neglect the exact size of the fluid lag. Furthermore, recent work [90] has demonstrated that in most practical situations the presence of the fluid lag is important only at the early time in the life of a hydraulic fracture: as the fracture evolves, the fluid lag tends to gradually disappear, specially under conditions of high confining stress (deep fractures). The explicit computation of the fluid lag can be replaced by the appropriate asymptotic behavior of width and pressure in the vicinity of the fracture front [40].

Work on the invaded zone case has not progressed to the point where clear conclusions can emerge. This is an area of current experimental and theoretical investigation (e.g., [68]).

3.6. Coupling

The elasticity, fluid flow, leak-off, fracture growth, and proppant transport equations should ideally all be fully coupled together in order to solve the system of equations correctly. In addition, pinch points may develop (e.g., due to the fracture growing in a higher stressed layer, or due to a region of the fracture becoming packed with proppant). Thus, it is necessary to implicitly couple a width constraint condition into the system of equations—a non-trivial task. It is also possible to couple in the effect of the evolving reservoir pore pressure distribution to the coupled elasto-hydrodynamic equations. Such schemes are preferential in high permeability situations where the leak-off may invade the reservoir ahead of the fracture tip and potentially dominate fracture growth.

In this section we discuss the algorithms that can be used to solve the discrete elasticity and fluid flow equations given by

$$Cw = p - \sigma_c, \tag{15a}$$

$$\frac{\Delta w}{\Delta t} = A(w)p + F \tag{15b}$$

for p and w. Here F contains the source and sink terms, C is the fully populated elasticity influence coefficient matrix and $A(w)$ is the sparse matrix that results from the discretization of $\nabla \cdot (D(w)\nabla \bullet)$, where, for simplicity, we restrict the discussion to Newtonian fluids. We assume that the fracture footprint has been established via some front location algorithm described above and that the time step Δt has been specified.

3.6.1. Explicit and implicit time stepping

Because of the non-linearity of the system of equations (15), it is tempting to use an explicit scheme to perform the time-stepping. However, the coupled system is particularly stiff as can be seen by the following illustrative example. If we consider the 1D KGD model, the discrete elasticity and fluid flow matrices have elements

$$C_{mn} = -\frac{E'}{4\pi\Delta x}\left[\frac{1}{(m-n)^2 - \frac{1}{4}}\right], \tag{16}$$

$$Ap_n = \frac{\bar{D}}{\Delta x^2}(p_{n+1} - 2p_n + p_{n-1}), \tag{17}$$

where E' is the elastic plane-strain modulus. Here we have used a collocation method to discretize the elastic integral equation assuming piecewise constant displacement discontinuity elements of length Δx. The nodal points at which the pressures and widths are sampled are located at element centers, which are assigned indices m and n. Standard central finite differences are used to discretize the fluid flow equations. In Eqs. (16) and (17), we have assumed that the width is slowly varying and is frozen to some nominal value $\bar{w}$, and that the conductivity $\bar{D}$ is thus defined as $\bar{D} = \bar{w}^3/12\mu$. Since both of these matrices are Toeplitz matrices (matrices with constant diagonals and for which $e^{ikn\Delta x}$ are eigenfunctions), it is possible to show [91] that the eigenvalues of the system matrix AC that governs

the evolution of the width vector are given by

$$\hat{A}_k \hat{C}_k = -\frac{2E'\bar{D}}{\Delta x^3}\sin^3\left(\frac{|k|\Delta x}{2}\right). \tag{18}$$

Thus if the explicit Euler method is used to evolve the solution to the system Eqs. (15a) and (15b) in which C and A are given by Eqs. (16) and (17), then stability dictates that the time step must satisfy the following CFL condition:

$$\Delta t < \frac{\Delta x^3}{E'\bar{D}}. \tag{19}$$

This CFL condition leads to prohibitively small time steps, each involving a multiplication by the fully populated matrix C. As a result of this extreme stiffness of the coupled equations, a backward Euler or some higher order backward difference scheme is recommended.

3.6.2. Picard iteration

In order to implement specially enhanced tip elements [85] it is necessary to use an algorithm that involves the inversion of C. Given a trial solution (w_k, p_k) a fixed point strategy based on this approach involves solving the fluid flow equation for p_{k+1}, which is then used in the elasticity equation to determine w_{k+1}. In order to stabilize this process the following sequence of Picard iterations are typically used:

$$\begin{aligned} p_{k+1/2} &= A(w_k)^{-1}\left(\frac{\Delta w_k}{\Delta t_k} - F\right),\\ p_{k+1} &= (1-\alpha)p_k + \alpha p_{k+1/2},\\ w_{k+1/2} &= C^{-1}(p_{k+1} - \sigma_c),\\ w_{k+1} &= (1-\alpha)w_k + \alpha w_{k+1/2}, \end{aligned} \tag{20}$$

where the invertability of A is ensured by imposing the solvability condition $\int_{\Omega(t)} \Delta w \, dV = Q\Delta t$. This process can be shown to converge for $0 < \alpha < \frac{1}{2}$ provided the time step is not too large and stress jumps or extreme changes in the elastic moduli are not encountered. However, if such extreme situations do occur then the Picard or similar schemes typically converge well initially but soon degenerate to spurious oscillations.

3.6.3. Newton iteration

On the other hand, Newton's method does not converge well if the initial guess is far from the solution but it converges very rapidly if the trial solution is close to the desired solution. In this case the Newton equations can be obtained by linearization of Eqs. (15a) and (15b) to yield the following system of linear equations:

$$\begin{bmatrix} -C & I \\ -\dfrac{1}{\Delta t}I + B_k & A_k \end{bmatrix} \begin{bmatrix} \delta w_k \\ \delta p_k \end{bmatrix} = - \begin{bmatrix} p_k - \sigma_c \\ A_k p_k + F - \dfrac{\Delta w_k}{\Delta t_k} \end{bmatrix}, \tag{21}$$

where I is the identity matrix, and

$$A_k = A(w_k), \quad B_k \approx \nabla \cdot (D'(w)\nabla p) \tag{22}$$

and the solution is subject to the following solvability condition:

$$\int_{\Omega(t)} \delta w_k \, dV = Q\Delta t - \int_{\Omega(t)} \Delta w \, dV. \tag{23}$$

Typically, an initial guess is determined by a few Picard iterations after which the coupling algorithm switches to a Newton scheme. If a pinch point develops during the iterative process then a width constraint of the form Eq. (2) must be imposed.

3.6.4. Proppant transport coupling

The proppant transport equations can be coupled to the elasto-hydrodynamic equations in a loose manner at the end of each time step. Given the latest width and pressure distributions from the simultaneous solution of Eqs. (15a) and (15b), we can determine the associated velocity field $\mathbf{v}^p$, which can be used in Eq. (12) to obtain the latest concentration distribution c. For each fracture element, we then update the local fluid properties as a function of the new c values and proceed to the next time step. Explicit solution of Eq. (12) necessitates a CFL restriction on the time-step. Since the front evolution is determined by implicit time stepping and pressure-width coupling, the front evolution time steps are typically much larger than the CFL restriction required in the solution of Eq. (12). The front evolution steps are therefore divided into sub-time-steps for the solution of Eq. (12), each of which satisfies the CFL restriction [92].

4. Application

To illustrate the complexity and the challenges involved in modeling hydraulic fracture treatments under real conditions, we present the following application example, based on real data. A hydrocarbon reservoir is located in two sandstone layers: the upper layer (Pay Zone 1) is located at a depth of 1615–1670 ft (492–509 m), and the lower layer (Pay Zone 2) at a depth of 2050–2150 ft (628–655 m), as shown in Fig. 9. Between these two "pay zones," there is an alternate array of layers of sandstone and shale, with varying stiffnesses and permeabilities. Downhole measurements yield a given interpretation of the elastic properties and the magnitude of the minimum confining stresses for the area surrounding the wellbore, as indicated in Fig. 9. Observation of the logs in Fig. 9 indicates the presence of relatively thin and stiff layers at various depths (these thin and hard layers are usually referred to as "streaks"). There are also two significant increments or jumps in the confining stress: a jump of 250 psi (1.7 MPa) at a depth of 2100 ft (640 m) (i.e., within Pay Zone 2), and a jump of 380 psi (2.6 MPa) at a depth of 2250 ft (686 m).

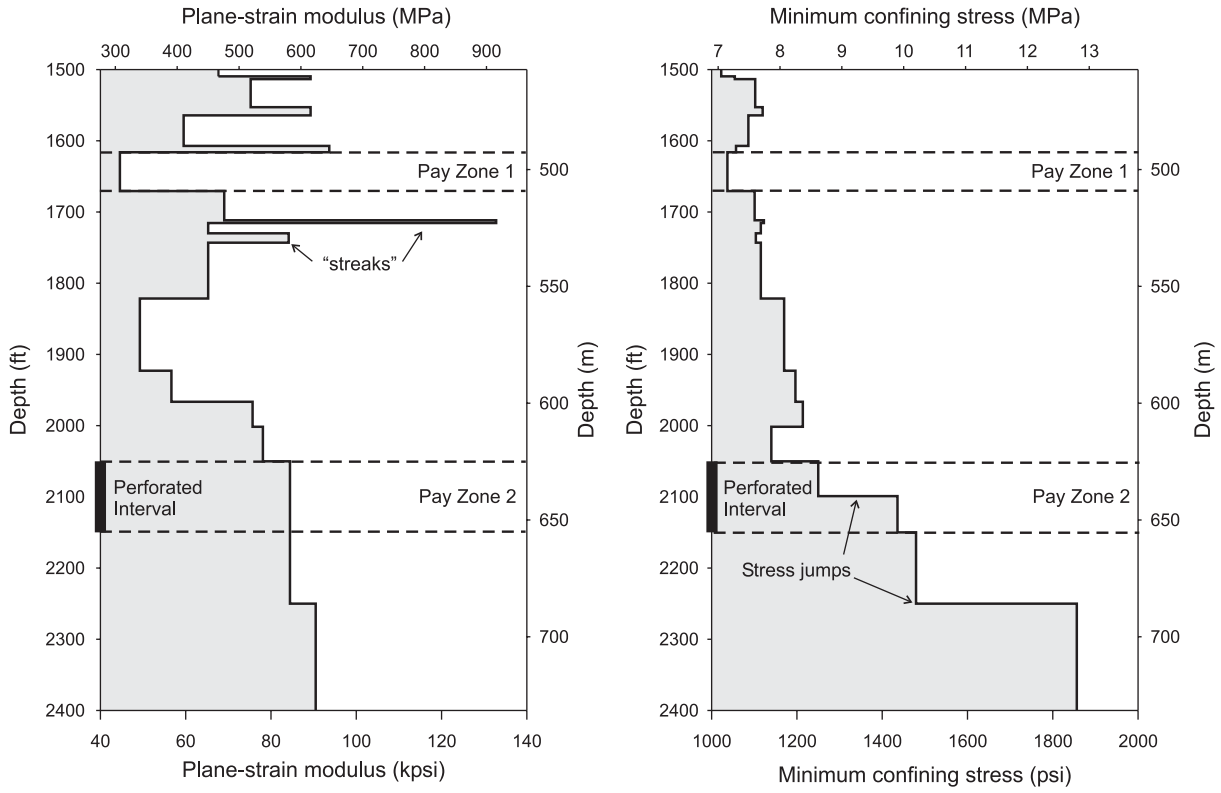

Fig. 9. Profiles of plane-strain modulus (left) and minimum *in situ* confining stress (right) versus depth.

The treatment design considers the perforated interval (i.e., the part of the wellbore from which the fracture will be initiated) to be located at Pay Zone 2. The sandstone in Pay Zone 1 is considered to be too weak for the wellbore casing to be perforated, as this would increase the risk of wellbore collapse or sanding. The design intends to take advantage of the bottom "stress barrier" to create a hydraulic fracture that would start in Pay Zone 2 and propagate upwards and connect to Pay Zone 1. It is also possible that the thin hard streaks may halt the fracture height growth.

The rock permeability is expressed in the fracture model in terms of the leak-off coefficient and spurt. In this particular case, the leak-off coefficient varies between 6.3×10^{-4} and $1.5 \times 10^{-3}\,\mathrm{ft/min^{1/2}}$ (2.4×10^{-5} and $5.9 \times 10^{-5}\,\mathrm{m/s^{1/2}}$), and the spurt for all the rock layers is assumed to be equal to $0.01\,\mathrm{gal/ft^2}$ ($4.1 \times 10^{-4}\,\mathrm{m^3/m^2}$).

The treatment design also considers a pumping schedule for both fluids and proppants. The schedule is shown in Fig. 10. An injection rate of 40 bbl/min ($0.11\,\mathrm{m^3/s}$) will be sustained for 120 min (7200 s). The first 60 min (3600 s) of the schedule is the "pad" of clean fluid. After 60 min of pumping, proppant is injected in incremental concentration stages, starting at 2 ppa ($c = 0.13$),[4] and increasing up to 12 ppa ($c = 0.48$). Pumping stops after 120 min, with a total injected VOF of 4157 bbl ($661\,\mathrm{m^3}$) and a total injected mass of proppant of 224 tons (203×10^3 kg). The period following pumping (in which the flow rate at the wellbore is kept to zero) is referred to as the "shut-in." During shut-in, the fluid contained in the fracture continues to leak off to the formation, and hence the observed pressure decline. Usually, fluid and proppant continue to mobilize (and the fracture continues to propagate) for a short period after shut-in starts. However, the fluid pressure in the fracture eventually equilibrates, rendering a practically null gradient of pressure everywhere, which essentially stops any further movement, except for gravity-induced settling. Shut-in continues until the fracture closes against the placed proppant. At this point, the net fluid pressure drops to zero, and it is considered that all the fracturing fluid[5] has leaked into the formation.

The selected fracturing fluid is a crosslinked HPG (hydroxypropylguar) polymer gel. This fluid has a power-law rheology defined[6] by an exponent $n' = 0.94$ and a consistency index $K' = 0.05\,\mathrm{lbf/ft^2\,s^{n'}}$ ($2.39\,\mathrm{Pa\,s^{n'}}$). The

[4]Proppant concentration is usually given in ppa units (pounds of dry proppant per gallon of clean fluid). The conversion formula between concentration in ppa and volumetric concentration c is

(*footnote continued*)

$c^{\mathrm{ppa}} = (c/(1-c))G_s\,\rho_w$, where G_s is the proppant solid's specific gravity, and ρ_w is the water density in pounds per gallon ($\rho_w \simeq 8.34$ lb/gal).

[5]In reality, part of the gel fraction of the fluid, plus the fluid trapped in the interstitial pores of the proppant pack remains in the fracture.

[6]These values of n' and K' are "nominal" values for clean fluid, usually measured at a given standard reference shear rate and temperature. During the simulation, these values are adjusted based on shear rate, temperature and proppant concentration.

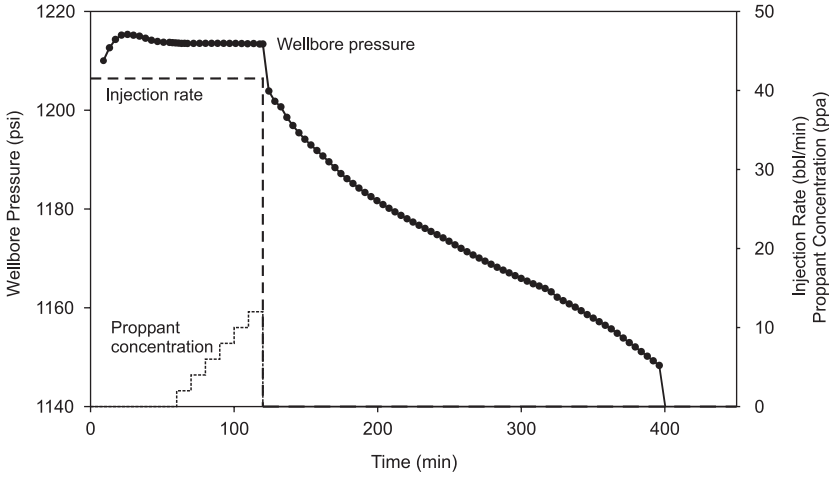

Fig. 10. Plot of treatment history.

selected proppant is a synthetic low-density proppant, with mean particle diameter of 0.025 in (0.64 mm) and solids specific gravity of 1.55.

Modeling of this treatment case was performed using a PL3D simulator with fixed (Eulerian) rectangular mesh and implicit time stepping. This simulator encompasses many of the features discussed in this paper. It uses a boundary integral scheme for solving the multi-layered elasticity equation, a finite difference scheme for the fluid flow equations, and a VOF method for iterating and tracking the fracture footprint. Fluid leak-off is calculated using the 1D Carter approximation. Proppant transport is modeled using an upwind method with a second-order limiter, and the fluid density and viscosity are adjusted depending upon the concentration of proppant. The mesh used in this particular case consisted of 65 horizontal $\times 35$ vertical rectangular elements, with a total horizontal extent of 2000 ft (610 m) and a total vertical extent of 820 ft (250 m). This simulator has been exhaustively (and successfully) tested against available analytical solutions for the penny-shaped [49] and PKN models [19,21], as well as laboratory experiments aimed to reproduce other effects, such as the crossing of stress barriers [93].

Results of the simulation are shown in Figs. 10–12. Fig. 10 shows the predicted evolution of fluid pressure at the wellbore with time, both during injection and after "shut-in." We observe that the model predicts a total closure of the fracture after 400 min of treatment time. Figs. 11 and 12, on the other hand, show "snapshots" of the fracture footprint (with contours of proppant concentration in ppa) and the fracture width profile at the wellbore, for different treatment times. At early time ($t = 9$ min), we observe that the fracture propagates within Pay Zone 2, but it is limited at the bottom by the first stress barrier. Towards the end of the pad injection ($t = 60$ min), the fracture has already propagated upwards (as expected). The important height growth explains the fact that the wellbore fluid pressure remains practically flat after an initial increase: if the fracture were to be contained within one single layer (i.e., as a PKN-type fracture), we would expect a monotonic increase of the pressure with time. At the end of the injection period ($t = 120$ min), the fracture has already reached Pay Zone 1, and it starts to propagate within this layer, confined from further height growth by a combination of stiffer elastic moduli and higher confinement at a depth of 1600 ft (488 m). The light proppant is carried up by the fluid, with minimum downward settling. Finally, at the end of shut-in ($t = 400$ min), the fracture is completely closed, and we observe a practically uniform distribution of proppant, with concentration of about 15 ppa ($c \simeq 0.5$), which ensures a good conductivity for the hydrocarbons between Pay Zone 1 and the perforated interval. We observe that the bottom stress barrier has been able to contain the fracture downwards. The fracture width profiles reflect the presence of the hard streaks and stress/modulus jumps.

5. Discussion

A number of open questions still need to be properly addressed in the modeling of hydraulic fractures. These include: (i) how best to address, in a numerically efficient and physically realistic manner, the handling of layer debonding and fluid invasion along layer interfaces with associated stunting of fracture height growth in shallower wells—relatively limited progress has been made in this area [94–96]; (ii) how to appropriately adjust current (linear elastic) simulators to enable modeling of the propagation of hydraulic fractures in highly cleated coal bed seams (for the extraction of methane) [97]; (iii) how to appropriately adjust current (linear elastic) simulators to enable modeling of the propagation of hydraulic fractures in weakly consolidated and unconsolidated "soft" sandstones, such as are found in the Gulf of Mexico—limited progress has been made in this area [98,99]; (iv) laboratory and field observations demonstrate that mode III fracture growth does occur [100], and this needs to be further researched;

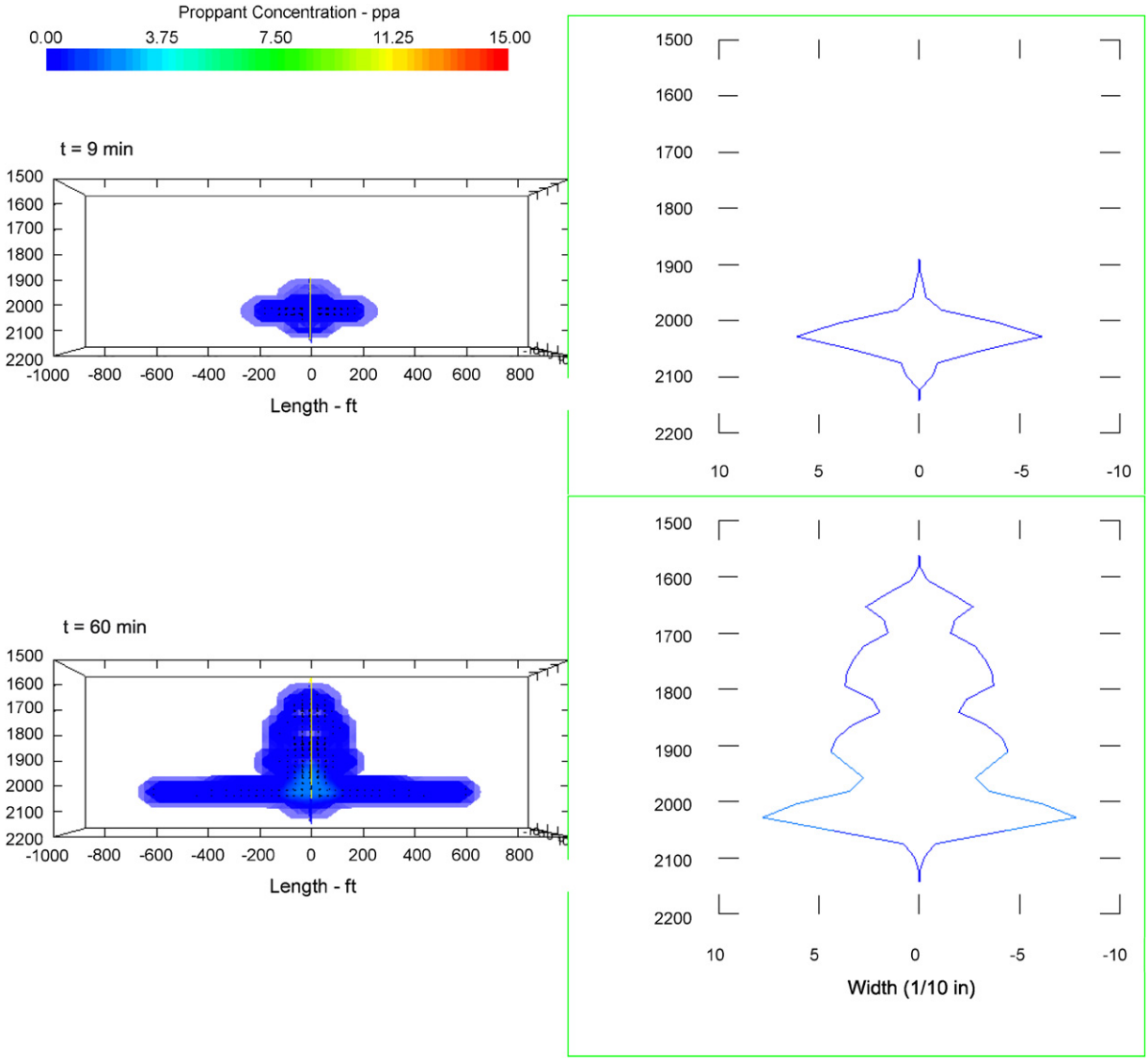

Fig. 11. Fracture footprint (left) showing contours of proppant concentration, and profiles of fracture width versus depth at the fracture center (right), at $t = 9$ and 60 min.

(v) related to (iii), the effect of the invaded zone ahead of the fracture tip needs to be further researched—a criterion to switch from a fluid lag based approach to an invaded zone based approach in a numerical model is required; (vi) suitable models for the propagation of hydraulic fractures in naturally fractured reservoirs that result in complex (non-planar) geometric configurations requires development [101]; and (vii) how to efficiently model 3D or "out of plane" effects, such as fracture re-alignment (when the fracture initiates following an orientation that is not perpendicular to the minimum *in situ* stress and then tries to re-align itself), which could be a cause of near-wellbore tortuosity or even "pinching," a factor that usually determines the success or failure of hydraulic fracturing treatments [102].

On the fluid mechanics side, the largest unknown is still the proper coupling of the rheology of the slurry to the rheology of the base fluid and the concentration and type of proppant. In particular, it is often assumed that the proppant particles travel at the same averaged speed as the fluid, which laboratory experiments have shown to be grossly incorrect [103–105].

There are also ongoing efforts to incorporate new fluids that do not follow standard power-law models into existing simulators, such as visco-elastic surfactants (VES) or polymeric fluids with complex time-, temperature- and/or shear-rate dependent properties. The development of improved leak-off models for these new fluids is also required, as well as improved models for use in high permeability situations (e.g., [106]) where leak-off can advance ahead of the fracture tip and no longer satisfies a 1D spatial model or follows a square root of time behavior [107].

With the advent of real-time micro-seismic, tiltmeter, and other monitoring during hydraulic fracturing treat-

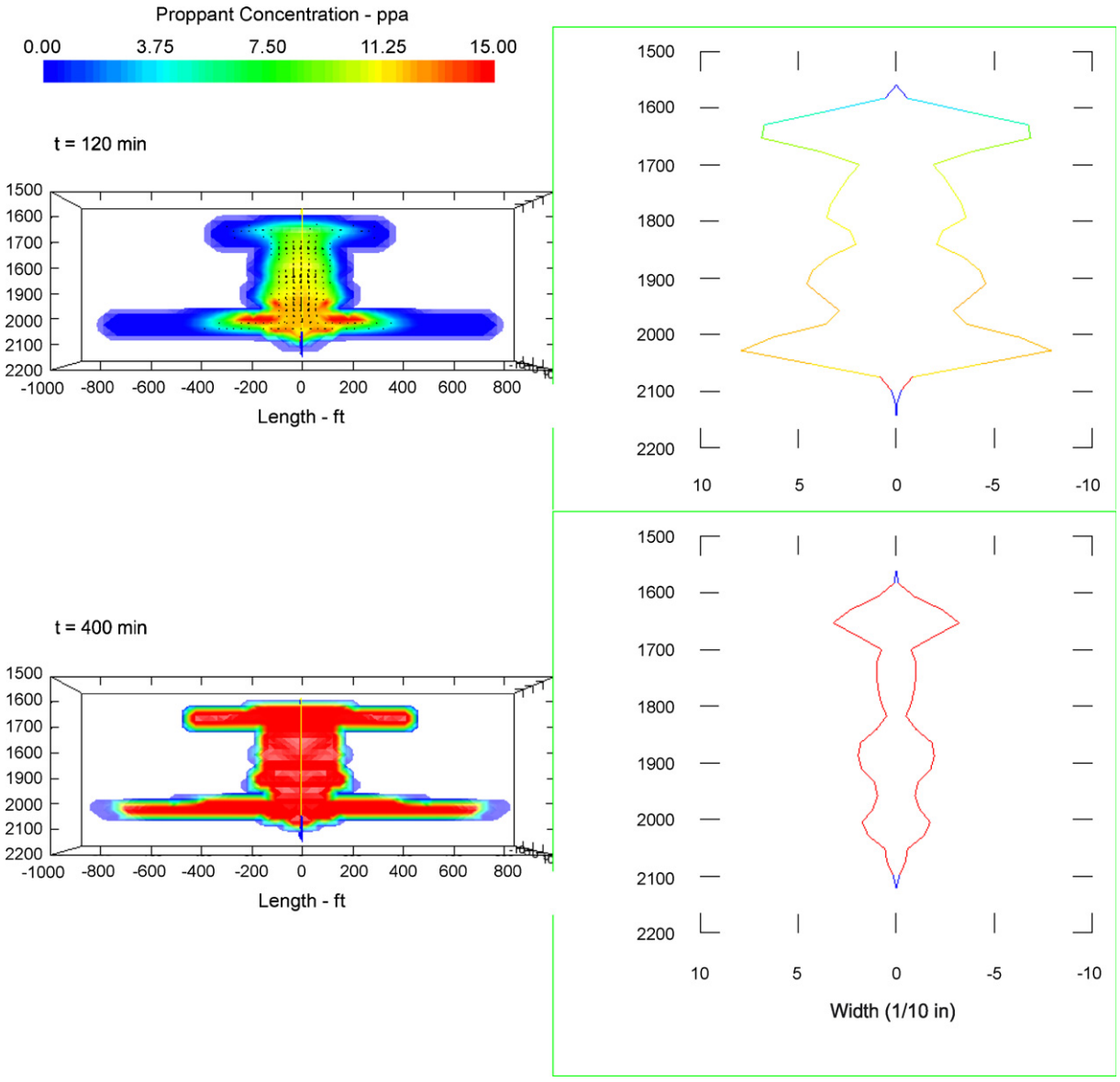

Fig. 12. Fracture footprint (left) showing contours of proppant concentration, and profiles of fracture width versus depth at the fracture center (right), at $t = 120$ and 400 min.

ments, there is a growing need for very fast models that can be used to update the treatment designs on the fly as information is fed back into the models. This is possible to do using existing P3D models, but PL3D models are still too CPU-intensive for practical use in such settings. Effort needs to be devoted to dramatically speed up PL3D simulators. Current fracture monitoring techniques often reveal a fracture shape more complex than a P3D model can adequately represent, and PL3D models can be used to extract more value from fracture monitoring activities.

The state of the art in hydraulic fracture modeling allows the petroleum industry to routinely design and evaluate stimulation treatments. It has not, however, reached a fully predictive capability which would allow for daring optimization strategies: today, most of the optimizations of stimulation treatments are based on an incremental strategy. Although we have focused on the forward modeling of hydraulic fractures, it is clear that a strong effort needs to be devoted to the inverse problem to develop robust methodologies to interpret limited field data and to make the best use of the available models to optimize fracturing treatments. Such an effort has been lacking whereas new monitoring methods have been developed and deployed in the field, and models have not yet been fully developed with such an inversion/optimization process in mind. The value-added step for the petroleum industry will be to have the models, the monitoring methods, and the inversion process tightly integrated so as to make the best use of all the efforts that have gone into developing hydraulic fracturing models over the past 50 years.

Acknowledgments

The authors thank Schlumberger for permission to publish, Hongren Gu for his contributions related to TVD-based methods for proppant transport, and Jack Elbel for his review of the historical background section of this paper. The first and second authors are indebted to Prof. Charles Fairhurst for providing encouragement during their studies at the University of Minnesota. His inspiration has ensured that the younger members of the *Minnesota Mafia* will continue to flourish for many years to come.

References

[1] Ptolemy (Claudius Ptolemæus). c. 130. The almagest. Book III [transl. R.C. Taliaferro. 1938. Encyclopædia Britannica, Inc. London. Repr. 1952].
[2] Lister JR. Buoyancy-driven fluid fracture: the effects of material toughness and of low-viscosity precursors. J Fluid Mech 1990;210: 263–80.
[3] Rubin AM. Propagation of magma-filled cracks. Ann Rev Earth Planet Sci 1995;23:287–336.
[4] Spence DA, Turcotte DL. Magma-driven propagation crack. J Geophys Res 1985;90:575–80.
[5] Moschovidis Z, et al. The Mounds drill-cuttings injection experiment: final results and conclusions. In: Proceedings of the IADC/SPE drilling conference, New Orleans, February 23–25. Richardson: Society of Petroleum Engineers; 2000 [SPE 59115].
[6] Pine RJ, Cundall PA. Applications of the Fluid-Rock Interaction Program (FRIP) to the modelling of hot dry rock geothermal energy systems. In: Proceedings of the international symposium on fundamentals of rock joints, Bjorkliden, Sweden, September 293–302, 1985.
[7] Zhang X, Detournay E, Jeffrey R. Propagation of a penny-shaped hydraulic fracture parallel to the free-surface of an elastic half space. Int J Fract 2002;115:126–58.
[8] Board M, Rorke T, Williams G, Gay N. Fluid injection for rockburst control in deep mining. In: Tillerson JR, Wawersik WR, editors. In: Proceedings of the 33rd U.S. symposium on rock mechanics. Rotterdam: Balkema; 1992. p. 111–20.
[9] Desroches J. Stress testing with the micro-hydraulic fracturing technique—focus on fracture reopening. In: Daemen JK, Schultz RA, editors. Proceedings of the 35th U.S. symposium on rock mechanics. Rotterdam: Balkema; 1995. p. 217–23.
[10] Grebe JJ, Stoesser M. Increasing crude production 20,000,000 bbl. from established fields. World Petroleum J 1935; (August):473–82.
[11] Frasch H. Increasing the flow of oil-wells. U.S. Patent Number 556669. United States Patents and Trademark Office. Washington DC; 1896.
[12] Watson TL. Granites of the Southeastern Atlantic States. Bulletin 426, U.S. Geological Survey, Washington DC, 1910.
[13] Veatch RW, Moschovidis ZA, Fast CR. An overview of hydraulic fracturing. In: Gidley, Holditch, Nierode, Veatch, editors. Recent advances in hydraulic fracturing. Monograph, vol. 12. Richardson: Society of Petroleum Engineers; 1989. p. 1–38.
[14] Crittendon BC. The mechanics of design and interpretation of hydraulic fracture treatments. J Pet Tech 1959; (October):21–9.
[15] Harrison E, Kieschnick WF, McGuire WJ. The mechanics of fracture induction and extension. Petroleum Trans AIME 1954; (201):252–63.
[16] Howard GC, Fast CR. Optimum fluid characteristics for fracture extension. Drilling Prod Pract 1957;24:261–70.
[17] Hubbert MK, Willis DG. Mechanics of hydraulic fracturing. J Pet Tech 1957;9(6):153–68.
[18] Khristianovic SA, Zheltov YP. Formation of vertical fractures by means of highly viscous liquid. In: Proceedings of the fourth world petroleum congress, Rome, 1955. p. 579–86.
[19] Perkins TK, Kern LR. Widths of hydraulic fractures. J Pet Tech 1961;13(9):937–49 [SPE 89].
[20] Sneddon IN, Elliot HA. The opening of a Griffith crack under internal pressure. Q Appl Math 1946;4:262–7.
[21] Nordren RP. Propagation of a vertical hydraulic fracture. SPE J 1972;12(8):306–14 [SPE 7834].
[22] Geertsma J, de Klerk F. A rapid method of predicting width and extent of hydraulically induced fractures. J Pet Tech 1969;21:1571–81 [SPE 2458].
[23] Sneddon IN. The distribution of stress in the neighbourhood of a crack in an elastic solid. Proc R Soc London A 1946;187:229–60.
[24] Green AE, Sneddon IN. The distribution of stress in the neighbourhood of a flat elliptical crack in an elastic solid. Proc Cambridge Philos Soc 1950;46:159–63.
[25] Daneshy AA. On the design of vertical hydraulic fractures. J Pet Tech 1973; (January):83–97 [SPE 3654].
[26] Spence DA, Sharp P. Self-similar solutions for elastohydrodynamic cavity flow. Proc R Soc London A 1985;400:289–313.
[27] Howard GC, Fast CR. Hydraulic fracturing. Monograph series, vol. 2. Richardson: Society of Petroleum Engineers; 1970.
[28] Simonson ER, Abou-Sayed AS, Clifton RJ. Containment of massive hydraulic fractures. SPE J 1978;18(1):27–32 [SPE 6089].
[29] Nolte KG, Smith MB. Interpretation of fracturing pressures. J Pet Tech 1981; (September):1767–75.
[30] Fung RL, Vilajakumar S, Cormack DE. Calculation of vertical fracture containment in layered formations. SPE Formation Eval 1987;2(4):518–23 [SPE 14707].
[31] Mack MG, Warpinski NR. Mechanics of hydraulic fracturing. In: Economides, Nolte, editors. Reservoir stimulation. 3rd ed. Chichester; Wiley: 2000 [Chapter 6].
[32] Advani SH, Lee TS, Lee JK. Three-dimensional modeling of hydraulic fractures in layered media: part I—finite element formulations. J Energy Resour Tech 1990;112:1–9.
[33] Ben Naceur K, Thiercelin M, Touboul E. Simulation of fluid flow in hydraulic fracturing: implications for 3D propagation. SPE Prod Eng J 1990; (May):133–41 [SPE 16032].
[34] Clifton RJ, Abou-Sayed AS. A variational approach to the prediction of the three-dimensional geometry of hydraulic fractures. In: Proceedings of the SPE/DOE low permeability symposium, Denver, May 27–29. Richardson: Society Petroleum Engineers; 1981 [SPE 9879].
[35] Clifton RJ, Wang J-J. Adaptive optimal mesh generator for hydraulic fracturing. In: Roegiers JC, editor. Rock mechanics as a multidisciplinary science. Rotterdam: Balkema; 1991. p. 607–16.
[36] Vandamme L, Curran JH. A three-dimensional hydraulic fracturing simulator. Int J Numer Meth Eng 1989;28:909–27.
[37] Barree RD. A practical numerical simulator for three-dimensional fracture propagation in heterogenous media. In: Proceedings of the SPE symposium reservoir simulation, San Francisco, November 15–18. Richardson: Society of Petroleum Engineers; 1983. p. 403–13 [SPE 12273].
[38] Siebrits E, Peirce AP. An efficient multi-layer planar 3D fracture growth algorithm using a fixed mesh approach. Int J Numer Meth Eng 2002;53:691–717.
[39] Carter BJ, Desroches J, Ingraffea AR, Wawrzynek PA. Simulating fully 3D hydraulic fracturing. In: Zaman M, Booker J, Gioda G, editors. Modeling in geomechanics. New York: Wiley Publishers; 2000.
[40] Desroches J, Detournay E, Lenoach B, Papanastasiou P, Pearson JRA, Thiercelin M, et al. The crack tip region in hydraulic fracturing. Proc R Soc London A 1994;447:39–48.
[41] Lenoach B. The crack tip solution for hydraulic fracturing in a permeable solid. J Mech Phys Solids 1995;43(7):1025–43.
[42] Detournay E, Adachi JI, Garagash D. Asymptotic and intermediate asymptotic behavior near the tip of a fluid-driven fracture

propagating in a permeable elastic medium. In: Dyskin A, Hu X, Sahouryeh E, editors. Structural integrity and fracture. Lisse; Swets & Zeitlinger: 2002. p. 9–18.
[43] Detournay E, Garagash D. The tip region of a fluid-driven fracture in a permeable elastic solid. J Fluid Mech 2003;494:1–32.
[44] Garagash DI, Detournay E. Near tip processes of a fluid-driven fracture. ASME J Appl Mech 2000;67:183–92.
[45] Detournay E. Propagation regimes of fluid-driven fractures in impermeable rocks. Int J Geomech 2004;4:1–11.
[46] Detournay E, Garagash D. Scaling laws for a radial hydraulic fracture propagating in a permeable rock. Proc R Soc London A, 2007, in preparation.
[47] Adachi JI, Detournay E. Self-similar solution of a plane-strain fracture driven by a power-law fluid. Int J Numer Anal Meth Geomech 2002;26:579–604.
[48] Carbonell RS, Desroches J, Detournay E. A comparison between a semi-analytical and a numerical solution of a two-dimensional hydraulic fracture. Int J Solids Struct 1999;36:4869–88.
[49] Savitski AA, Detournay E. Propagation of a fluid-driven penny-shaped fracture in an impermeable rock: asymptotic solutions. Int J Solids Struct 2002;39:6311–37.
[50] Garagash DI, Detournay E. Plane-strain propagation of a hydraulic fracture: small toughness solution. J Appl Mech 2005;72(6): 916–28.
[51] Adachi JI, Detournay E. Plane-strain propagation of a fluid-driven fracture: finite toughness self-similar solution. Int J Fracture 2007, to be submitted.
[52] Garagash DI. Plane strain propagation of a hydraulic fracture during injection and shut-in: large toughness solutions. Eng Frac Mech 2006;73(4):456–81.
[53] Adachi JI, Detournay E. Plane-strain propagation of a fluid-driven fracture in a permeable medium. Eng Frac Mech 2007, submitted.
[54] Mitchell SL, Kuske R, Peirce AP. An asymptotic framework for finite hydraulic fractures including leak-off. SIAM J Appl Math 2007, in press.
[55] Bunger A. Near-surface hydraulic fracture. PhD thesis, University of Minnesota, Minneapolis; 2005.
[56] Bunger A, Detournay E, Jeffrey R. Crack tip behavior in near-surface fluid driven fracture experiments. C Re Mech 2005;333: 299–304.
[57] Lhomme T. Initiation of hydraulic fractures in natural sandstones. PhD thesis, Delft University of Technology, Delft; 2005.
[58] Starfield AM, Cundall PA. Towards a methodology for rock mechanics modelling. Int J Rock Mech Min Sci Geomech Abstr 1988;25(3):99–106.
[59] Peirce AP, Siebrits E. Uniform asymptotic approximations for accurate modeling of cracks in layered elastic media. Int J Fracture 2002;110:205–39.
[60] Peirce AP, Siebrits E. The scaled flexibility matrix method for the efficient solution of boundary value problems in 2D and 3D layered elastic media. Comput Methods Appl Mech Eng 2001;190(45): 5935–56.
[61] Crouch SL, Starfield AM. Boundary element methods in solid mechanics. London: Unwin & Hyman; 1990.
[62] Du Y, Segall P, Gao H. Dislocations in inhomogeneous media via a moduli perturbation approach: general formulation and two-dimensional solutions. J Geophys Res 1994;99(B7):767–79.
[63] Guddati MN, Tassoulas JL. Space-time finite elements for the analysis of transient wave propagation in unbounded layered media. Int J Solids Struct 1999;36:4699–723.
[64] Shou KJ, Napier JAL. A two-dimensional linear variation displacement discontinuity method for three-layered elastic media. Int J Rock Mech Min Sci 1999;36:719–29.
[65] Wang J-J, Clifton RJ. Numerical modeling of hydraulic fracturing in layered formations with multiple elastic moduli. In: Hustrulid, Johnson, editors. Rock mechanics contributions and challenges. Rotterdam: Balkema; 1990. p. 303–10.
[66] Napier JAL. Personal communications, 1999.
[67] Miskimins JL, Barree RD. Modeling of hydraulic fracture height containment in laminated sand and shale sequences. In: Proceedings of the SPE production and operations symposium, Oklahoma City, March 22–25. Richardson: Society of Petroleum Engineers; 2003 [SPE 80935].
[68] Khodaverdian M, McElfresh P. Hydraulic fracturing stimulation in poorly consolidated sand: mechanisms and consequences. In: Proceedings of the 75th SPE annual technical conference and exhibition, Dallas, October 1–4. Richardson: Society of Petroleum Engineers; 2000 [SPE 63233].
[69] Seright RS. An alternative view of filter cake formation in fractures. In: Proceedings of the 13th SPE/DOE improved oil recovery symposium, Tulsa, April 13–17. Richardson: Society of Petroleum Engineers; 2002 [SPE 75158].
[70] Calhoun D, LeVeque RJ. A Cartesian grid finite-volume method for the advection-diffusion equation in irregular geometries. J Comput Phys 2000;157:143–80.
[71] Drew DA, Passman SL. Theory of multicomponent fluids. Applied mathematical sciences, vol. 134. New York: Springer; 1999.
[72] Clark P, Quadir J. Proppant transport in hydraulic fractures: a critical review of particle settling velocity equations. In: Proceedings of the SPE/DOE low permeability symposium Denver, May 27–29. Richardson: Society of Petroleum Engineers; 1981. p. 343–7 [SPE 9866].
[73] Hammond P. Settling and slumping in a Newtonian slurry, and implications for proppant placement during hydraulic fracturing of gas wells. Chem Eng Sci 1995;50(20):3247–60.
[74] Pearson JRA. On suspension transport in a fracture: framework for a global model. J Non-Newtonian Fluid Mech 1994;54:503–13.
[75] Hirsch C. Numerical computation of internal and external flows, volume 2: computational methods for inviscid and viscous flows. New York: Wiley; 1990.
[76] LeVeque RJ. Finite volume methods for hyperbolic problems. Cambridge: Cambridge University Press; 2002.
[77] Sweby PK. High-resolution schemes using flux limiters for hyperbolic conservation laws. SIAM J Numer Anal 1984;21:995–1011.
[78] Clifton RJ, Wang J-J. Multiple fluids, proppant transport, and thermal effects in three-dimensional simulation of hydraulic fracturing. Proceedings of the 63rd SPE annual technical conference and exhibition, Houston, October 2–5, 1988. p. 175–88 [SPE 18198].
[79] Daneshy AA. Numerical solution of sand transport in hydraulic fracturing. J Pet Tech 1978; 132–40 [SPE 5636].
[80] Novotny EJ. Proppant transport. In: Proceedings of the 52nd SPE annual technical conference and exhibition, Denver, October 9–12. Richardson: Society of Petroleum Engineers; 1977 [SPE 6813].
[81] Barree RD, Conway M. Experimental and numerical modeling of convective proppant transport. In: Proceedings of 69th SPE annual technical conference and exhibition, New Orleans, September 25–28. Richardson: Society of Petroleum Engineers; 1994. p. 531–46 [SPE 28564].
[82] Nolte KG. Fluid flow considerations in hydraulic fracturing. In: Proceedings of the SPE eastern regional meeting, Charleston, November 1–4. Richardson: Society of Petroleum Engineers; 1988. p. 145–56 [SPE 18537].
[83] Shah S. Rheological characterization of hydraulic fracturing slurries. In: Proceedings of the 66th SPE annual technical conference and exhibition, Dallas, October 6–9, Richardson: Society of Petroleum Engineers; 1991. p. 229–42 [SPE 22839].
[84] Fedorenko RP. Some problems and approximate methods of computational mechanics. Comp Meth Math Phys 1994;34(2): 223–41.
[85] Napier JAL, Stephansen SJ, Analysis of deep-level mine design problems using the MINSIM-D boundary element program. In: Proceedings of the 20th international symposium on the application of computers and mathematics in the mineral industries, vol. 1. SAIMM; 1987; p. 3–19.
[86] Hirt CW, Nichols BD. Volume of fluid (VOF) method for the dynamics of free boundaries. J Comput Phys 1981;39:201–25.

[87] Osher S, Sethian J. Fronts propagating with curvature-dependent speed: algorithms based on Hamilton–Jacobi formulations. J Comput Phys 1988;79:12–49.
[88] Sethian JA. Level set methods. Cambridge: Cambridge University Press; 1998.
[89] SCR Geomechanics Group. On the modelling of near tip processes. Int J Rock Mech Min Sci 1994; 30(7):1127–34.
[90] Garagash DI. Propagation of a plane-strain fluid-driven fracture with a fluid lag: early-time solution. Int J Solids Struct 2006;43: 5811–35.
[91] Peirce AP, Siebrits E. A dual mesh multigrid preconditioner for the efficient solution of hydraulically driven fracture problems. Int J Numer Meth Eng 2005;63(13):1797–1823.
[92] Gu H, Siebrits E. On numerical solutions of hyperbolic proppant transport problems. In: Proceedings of the 10th international conference on hyperbolic problems: theory, numerics and applications, Osaka, Japan, September 13–17, 2004.
[93] Jeffrey RG, Bunger A. A detailed comparison of experimental and numerical data on hydraulic fracture height growth through stress contrasts. In: Proceedings of the 2007 SPE hydraulic fracturing technology conference, College Station, January 29–31, 2007 [SPE 106030].
[94] Barree RD, Winterfeld PH. Effect of shear planes and interfacial slippage on fracture growth and treating pressure. Proceedings of the 73rd SPE annual technical conference and exhibition, New Orleans, September 27–30. Richardson: Society of Petroleum Engineers; 1998 [SPE 48926].
[95] Zhang X, Jeffrey RG. The roles of secondary flaws and friction on deflection and reinitiation of hydraulic fractures at orthogonal pre-existing fractures. Geophys J Int 2006;166:1454–65.
[96] Zhang X, Jeffrey RG, Thiercelin M. Deflection and propagation of fluid-driven fractures at frictional bedding interfaces: a numerical investigation, J Struct Geol 2007, accepted for publication.
[97] Olsen TN, Brenize G, Frenzel T. Improvement processes for coalbed natural gas completion and stimulation. In: Proceedings of the 79th SPE annual technical conference and exhibition, Denver, October 5–8. Richardson: Society of Petroleum Engineers; 2003 [SPE 84122].
[98] Smith MB, et al. High-permeability fracturing: "Carter" fluid loss or not. In: Proceedings of the SPE international symposium and exhibition on formation damage control, Lafayette, February 18–20. Richardson: Society of Petroleum Engineers; 2004 [SPE 86550].
[99] van Dam DB, Papanastasiou P, de Pater CJ. Impact of rock plasticity on hydraulic fracture propagation and closure. In: Proceedings of the 76th SPE annual technical conference and exhibition, Dallas, October 1–4. Richardson: Society of Petroleum Engineers; 2000 [SPE 63172].
[100] Germanovich L, Astakhov D. Multiple fracture model. In: Jeffrey, McLennan, editors. Proceedings of the three dimensional and advance hydraulic fracture modeling. Workshop held at 4th North American rock mechanics symposium, Seattle, July 29–31, 2000. p. 45–70. ⟨http://www.dpr.csiro.au/people/rob/HFWorkshopSeattle2000.pdf⟩
[101] Maxwell SC, Urbancic TI, Steinsberger N, Zinno R. Microseismic imaging of hydraulic fracture complexity in the Barnett Shale. In: Proceedings of the 78th SPE annual technical conference and exhibition, San Antonio, September 29–October 2. Richardson: Society of Petroleum Engineers; 2002 [SPE 77440].
[102] Romero J, Mack MG, Elbel JL. Theoretical model and numerical investigation of near-wellbore effects in hydraulic fracturing. In: Proceedings of the SPE annual technical conference and exhibition, Dallas, October 22–25. Richardson: Society of Petroleum Engineers; 1995 [SPE 30506].
[103] Abbott JR, Tetlow N, Graham AL, Altobelli SA, Fukushima E, Mondy LA, et al. Experimental observations of particle migration in concentrated suspensions: Couette flow. J Rheol 1991;35(5): 773–86.
[104] Tehrani MA. An experimental study of particle migration in pipe flow of viscoelastic fluids. J Rheol 1996;40(6):1057–77.
[105] Tetlow N, Graham AL, Ingber MS, Subia SR, Mondy LA, Altobelli A. Particle migration in a Couette apparatus: experiment and modeling. J Rheol 1998;42(2):307–27.
[106] van den Hoek PJ. A simple and accurate description of nonlinear fluid leak-off in high-permeability fracturing. SPE J 2002; (March):14–23 [SPE 77183].
[107] Murdoch LC, Germanovich LN. Analysis of a deformable fracture in permeable material. Int J Numer Anal Meth Geomech 2006;30: 529–61.
[108] Desroches J, Thiercelin M. Modeling propagation and closure of micro-hydraulic fracturing. Int J Rock Mech Min Sci 1993;30: 1231–4.